

Electronic Supplementary Information

Wavelength dependent luminescence decay kinetics in ‘quantum-confined’g- C₃N₄ nanosheets exhibiting high photocatalytic efficiency upon plasmonic coupling

Sanjit Mondal¹, Lipipuspa Sahoo¹, Yuvraj Vaishnav¹, Samita Mishra¹, Raj Sekhar Roy¹, C. P.
Vinod², Arijit K De¹, Ujjal K. Gautam^{1,*}

¹Department of Chemical Sciences, Indian Institute of Science Education and Research (IISER)-Mohali, Sector 81,
Mohali, SAS Nagar, Punjab 140306, India

²Catalysis and Inorganic Chemistry Division, CSIR-NCL, Pune 411008, India

**Corresponding author: ujjalgautam@iisermohali.ac.in, ujjalgautam@gmail.com*

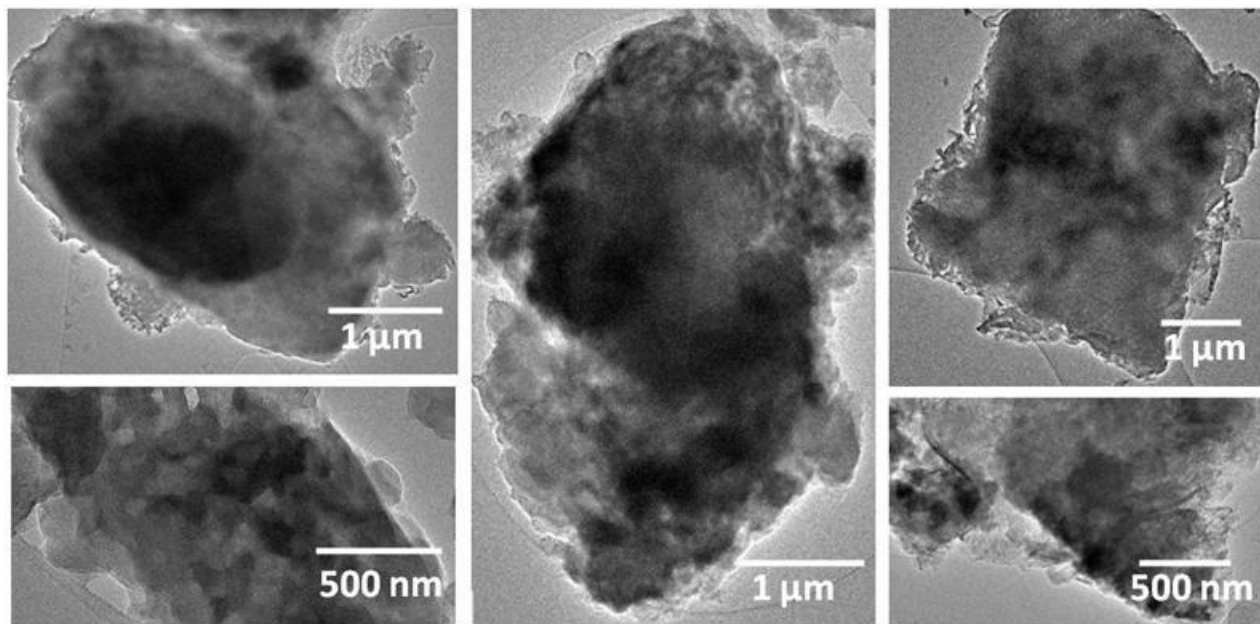


Fig. S1 TEM images of the settled g-C₃N₄ powder after sonication. The images at various magnifications show that these are somewhat bigger and thicker than the nanosheets.

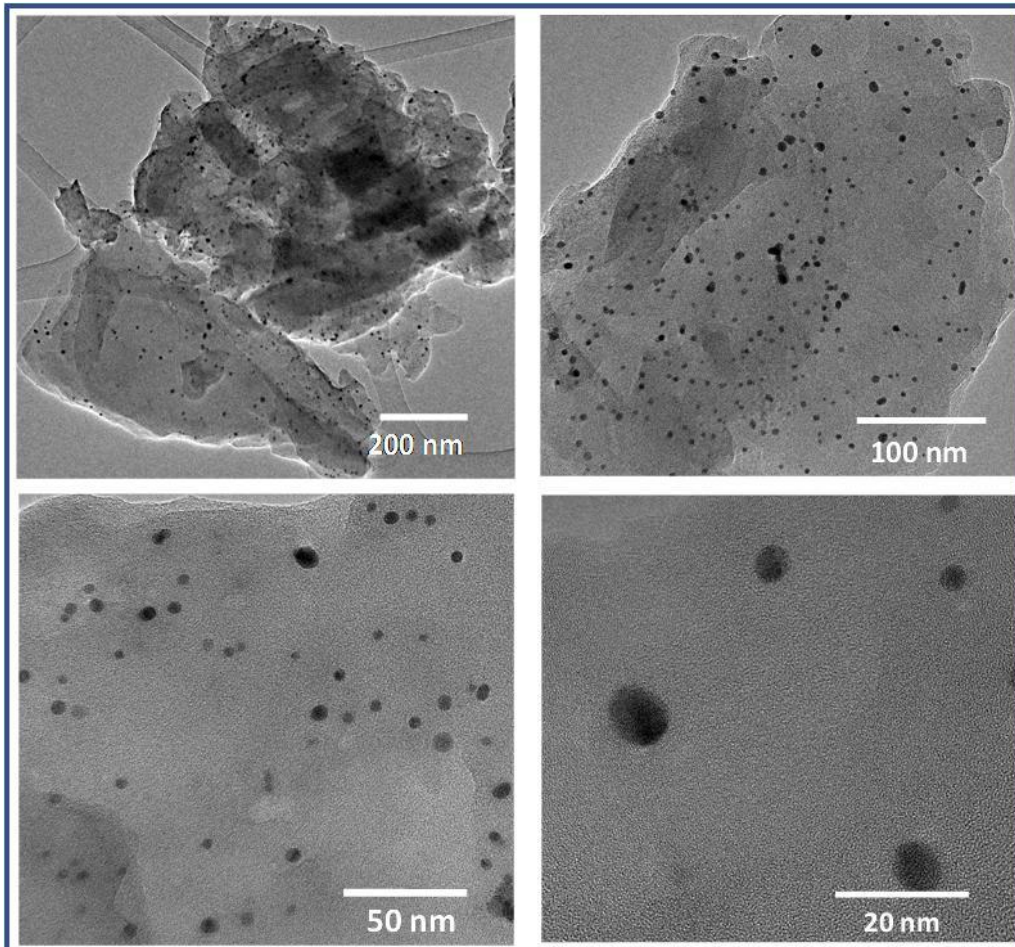


Fig. S2 TEM images of Au/g-C₃N₄ nanosheets at different magnifications.

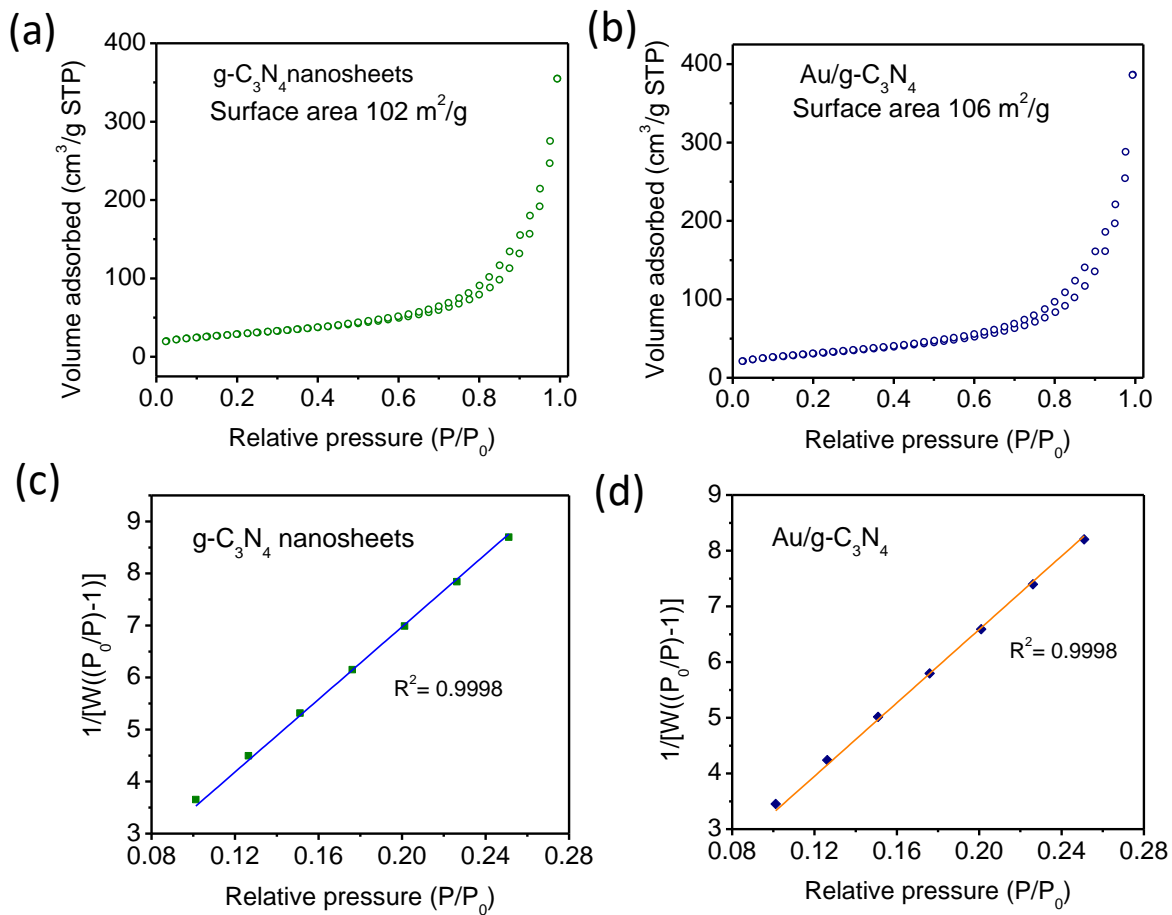


Fig. S3 N_2 gas adsorption-desorption plots for pure $g\text{-C}_3\text{N}_4$ nanosheets (a), and $\text{Au}/g\text{-C}_3\text{N}_4$ nanosheets (b). Multi-point BET surface area plots for pure $g\text{-C}_3\text{N}_4$ nanosheets (c) and $\text{Au}/g\text{-C}_3\text{N}_4$ nanosheets (d).

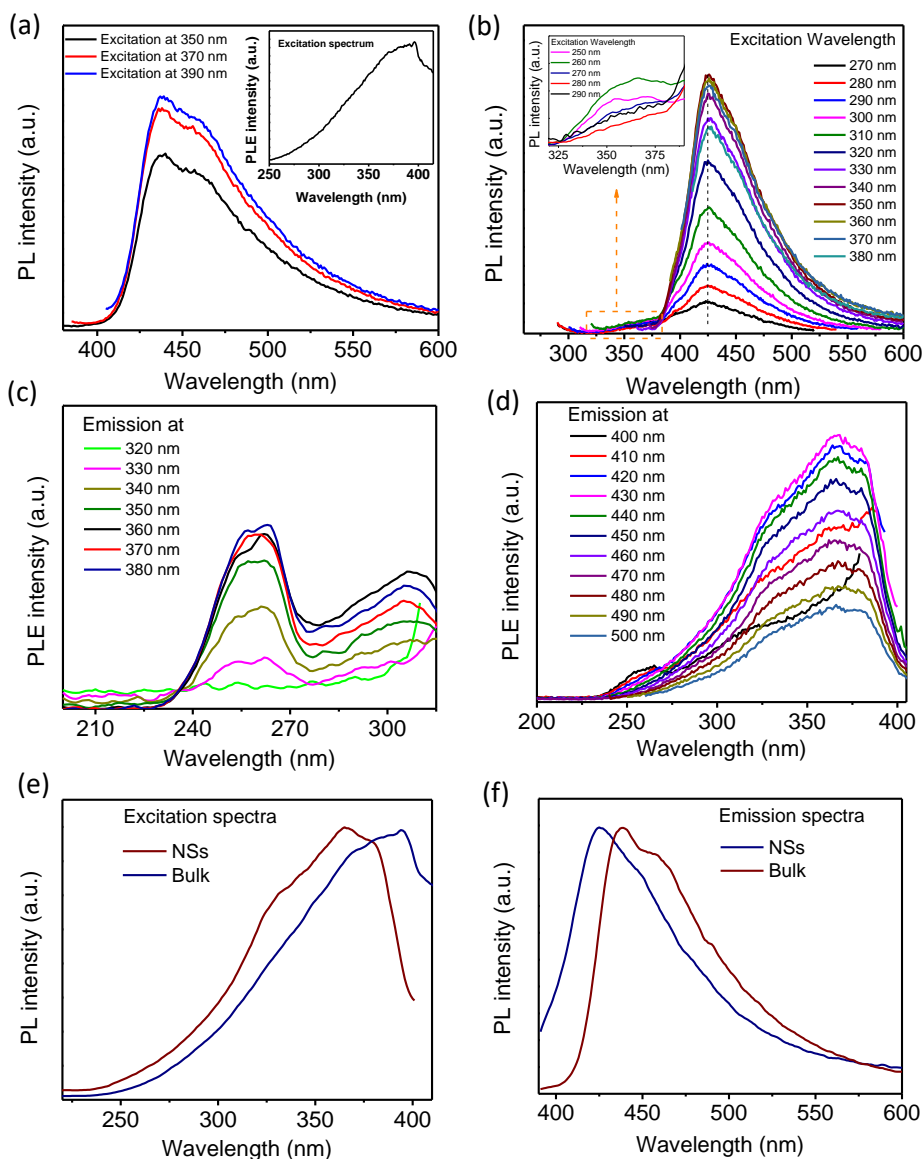


Fig. S4 (a) PL spectra of as-prepared $g\text{-C}_3\text{N}_4$ sample showing the emission maxima at ~ 440 nm with 390 nm excitation wavelength. The inset of (a) is the corresponding PLE spectrum. (b) The PL spectra of $g\text{-C}_3\text{N}_4$ nanosheets at different excitation wavelengths, showing the unshifted emission maxima at ~ 425 nm. Inset shows a tiny PL peak emerging at ~ 370 nm corresponding to a trace amount of melem present in the sample. (c, d) The PLE spectra of $g\text{-C}_3\text{N}_4$ nanosheets at different emission wavelengths corresponding to the nanosheets and tiny fraction of melem, showing that the two peaks originate broadly of independent excitations. Notably there is a distinct shift in the PLE spectra of the as-prepared sample and the nanosheets. PL excitation (e) and emission spectra (f) of bulk and nanosheets of $g\text{-C}_3\text{N}_4$.

Note S1: A weak emission band centered at 370 nm was also observed in the PL spectra of g-C₃N₄ nanosheets (inset in Fig. S4), suggesting the presence of melem traces along with g-C₃N₄.¹ The PLE maxima for this melem emission were found at ~260 nm (Fig. S4c). The corresponding emission spectra were given in Fig. S4c.

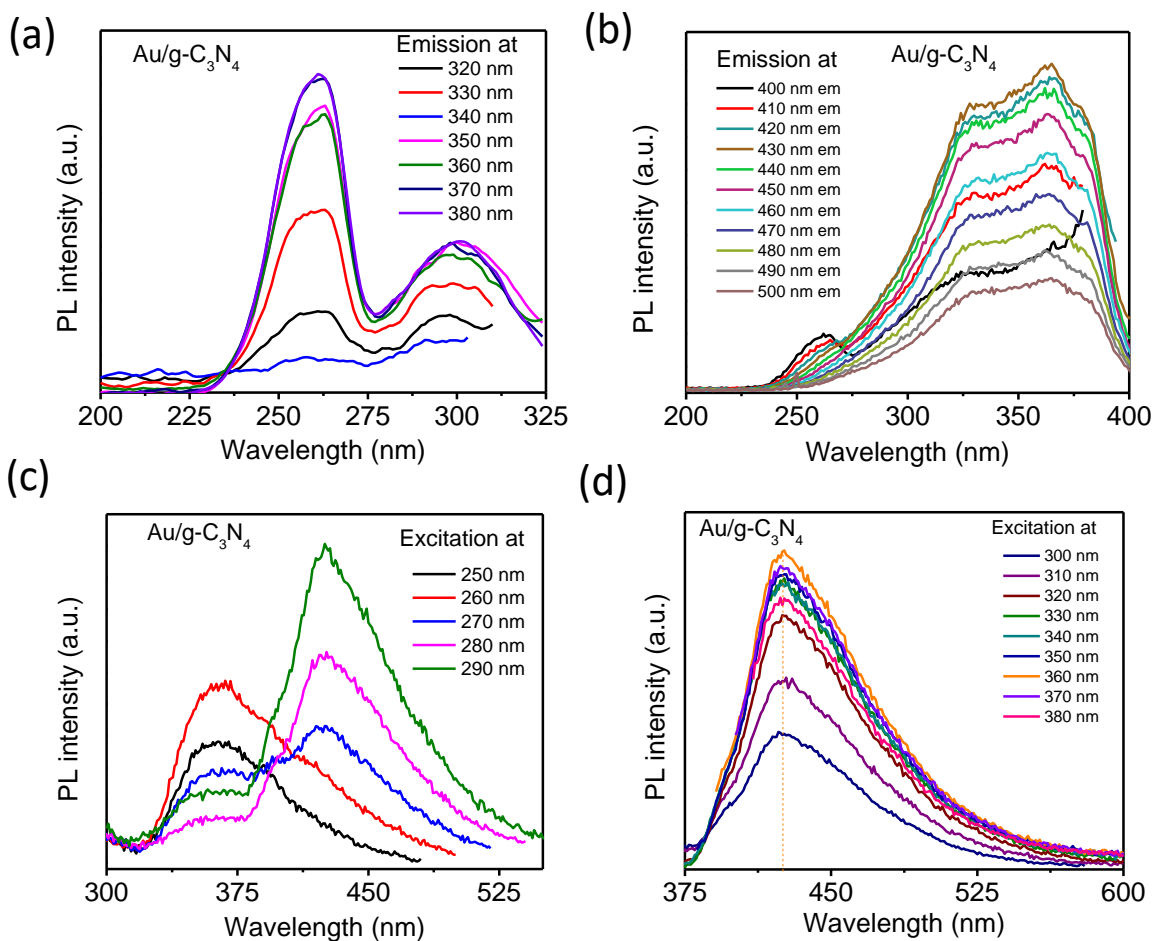


Fig. S5 PLE spectra of Au/g-C₃N₄ nanosheets at different emission energies (a, b). The PL emission spectra of Au/g-C₃N₄ nanosheets at different excitation wavelength (c, d). The peak position remained same (~425 nm) at all excitation wavelengths.

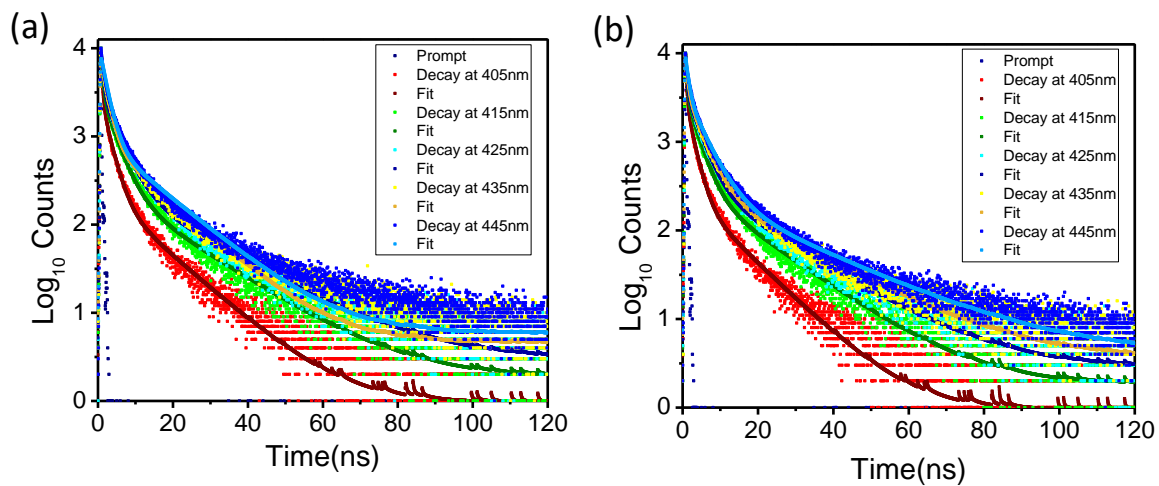


Fig. S6 Typical TCSPC decay plots of g-C₃N₄ and Au/g-C₃N₄ nanosheets at different emission wavelengths when excited with a 375 nm laser.

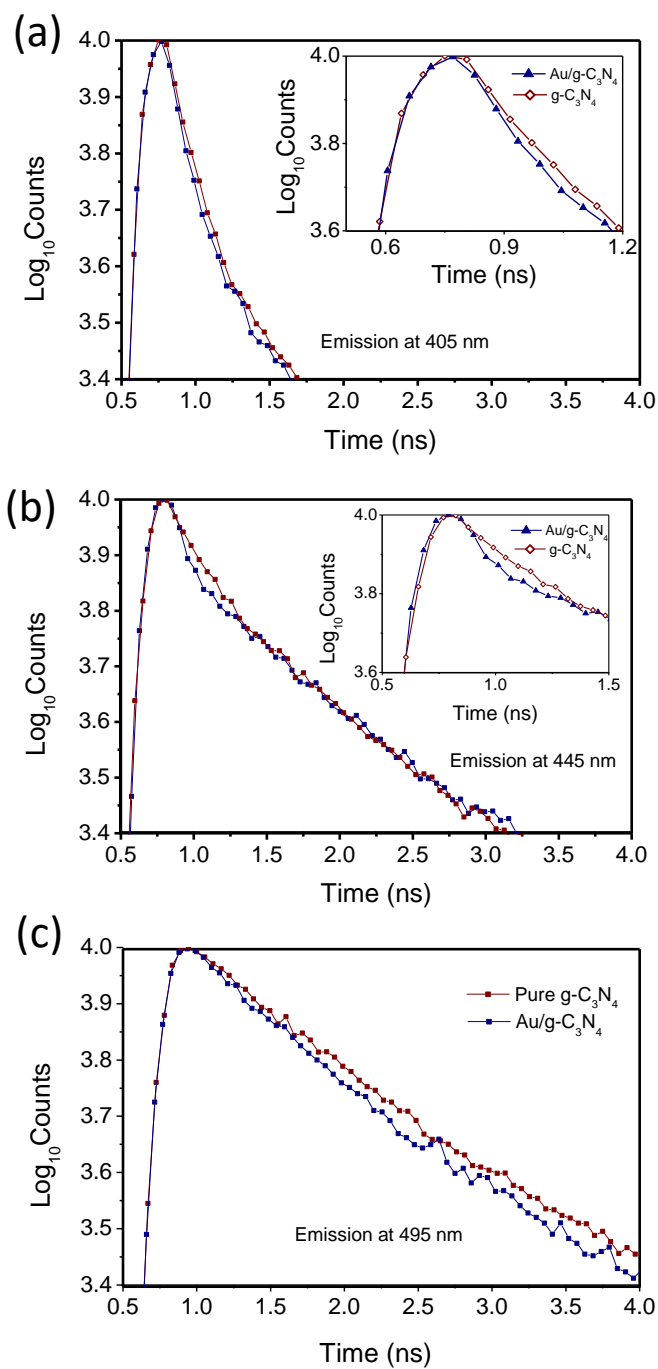


Fig. S7 The time-resolved fluorescence decay plots for pure and Au loaded nanosheets at 405 nm (a), 445 nm (b) and 495 nm (c) within the first few nanoseconds.

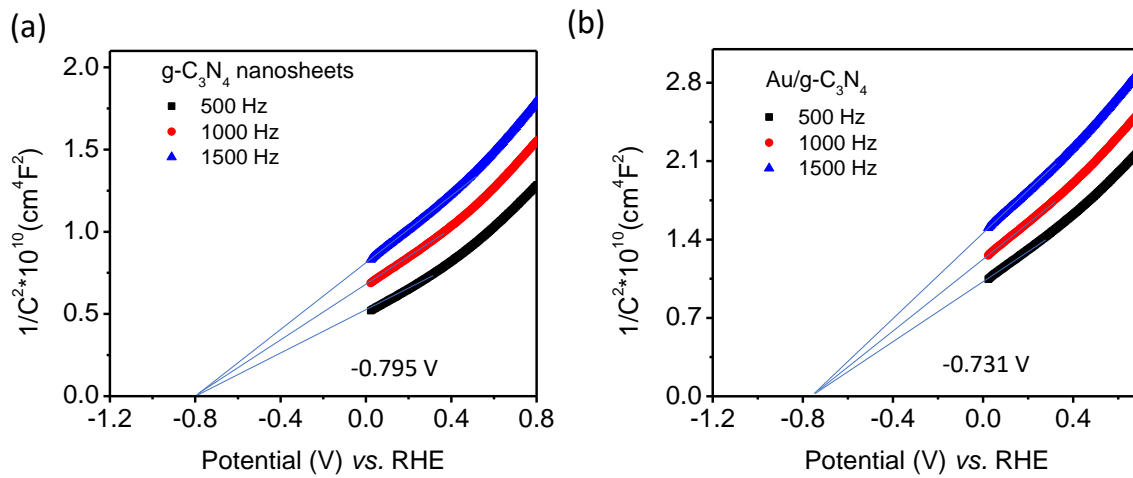


Fig. S8 Mott-Schottky plots for the nanosheets of $g\text{-C}_3\text{N}_4$ (a) and $\text{Au/g-C}_3\text{N}_4$ (b).

Note S2. Calculation of Apparent Quantum Efficiency (AQE): In order to calculate the AQE for the photocatalytic benzyl amine oxidation, we considered the reaction in direct sunlight with a reaction yield of 98% in 1.5 h and the solar spectrum at the sea-level (Figure S9). Since, sun-light intensity may slightly vary and hence the calculated AQE can be considered representative, with a minimal deviation from expected values. For the calculation of overall efficiency, we counted the number of incident photons from higher energies till 800 nm where, based on the UV-Vis absorption spectrum of Au/g-C₃N₄, the absorption is >93%.² We have also calculated the number of photon in the range of 400-800 nm for solar simulator and 300-800 nm in case of solar spectrum. The AQE we report below, in all probability, is smaller than the actual quantum efficiency as the number of absorbed photons is expected to be lesser than that of incident ones. The incident power on the sample can be represented as:

$$P_{\text{incident}} = \rho_{\text{incident}}(\lambda) \times A_{\text{sample}}$$

A_{sample} is the area exposed to incident light (12 cm²), $\rho_{\text{incident}}(\lambda)$ is the incident power on the sample corresponding to photon of wavelength λ .

The incident powers on the sample was estimated to be 775 and 560 mW in the wavelength range of 300-800 nm for solar spectrum and 400-800 nm for solar simulator respectively. The number of incident photons per second, as a function of wavelength can be expressed as:

$$N_{ph}(\lambda) = \frac{\rho_{\text{incident}}(\lambda)}{E_{ph}(\lambda)}$$

Where $E_{ph}(\lambda) = hc/\lambda$ is the photon energy for the corresponding wavelength. For example, the total number of photons incident on the sample per second within wavelength range of 300-800 nm can be calculated as:

$$N_{ph,incident}(300 - 800) = \int_{300}^{800} \frac{\rho_{\text{incident}}(\lambda) \times \lambda}{hc} d\lambda$$

The AQE can be derived from the following equation:

$$AQE = n (\text{No. of electron or hole}) \times \frac{\text{Number of imine molecule produced}}{\text{Number of incident photons}} \times 100 (\%)$$

For benzyl amine oxidation n is 2.

(For 300-800 nm) solar spectrum:

$$AQE = 2 \times \frac{0.00049}{0.0158} \times 100(\%) = 6.22 \%$$

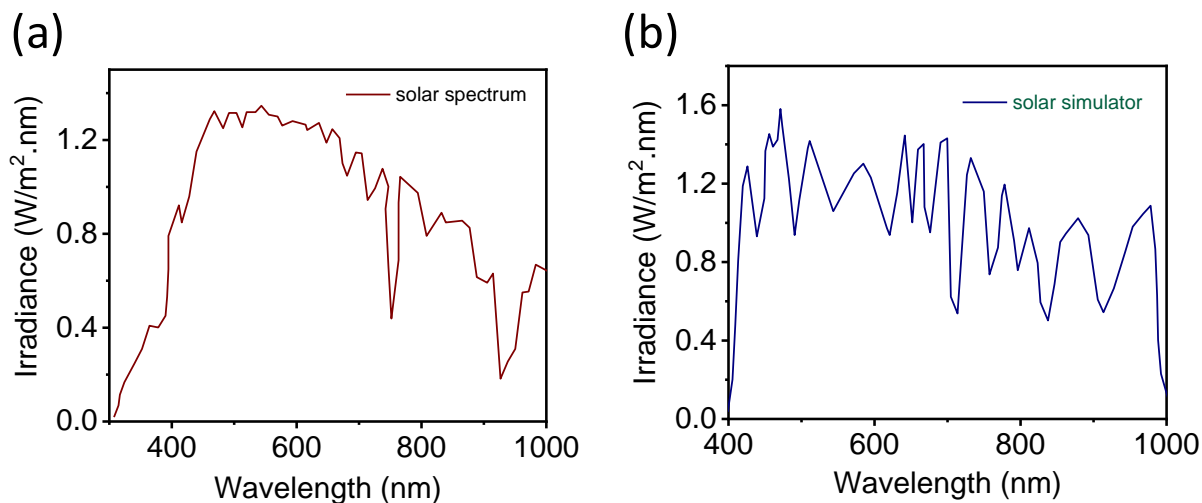


Fig. S9 (a) Solar spectrum at sea-level and (b) solar-simulator spectrum used for calculating apparent quantum efficiencies.

Estimation of co-catalytic contribution done in the following manner: After 1.5 h of reaction in the

			<u>Difference</u>
300-800 nm (direct sun)	0.125 mmol (bare)	& 0.490 mmol (Au/gC3N4)	
400-800 nm (LED solar)	0.063 mmol (bare)	& 0.285 mmol (Au/gC3N4)	=> 0.222 mmol
			(mainly SPR enhanced)

Since the spectra in 400-800 & 300-800 nearly overlap,

300-400 nm	0.062 mmol (bare)	& 0.205 mmol (Au/gC3N4)	=> 0.143 mmol
			(mainly co-catalytically enhanced)

Total enhancement = 0.222 mmol + 0.143 mmol = 0.365 mmol

Approximate co-catalytic enhancement = ~38%

Note that the improvement in the 400-500 nm region is contributed by both co-catalytic and plasmonic factors. Consequently, we suspect 3-5% variation in co-catalytic contributions.

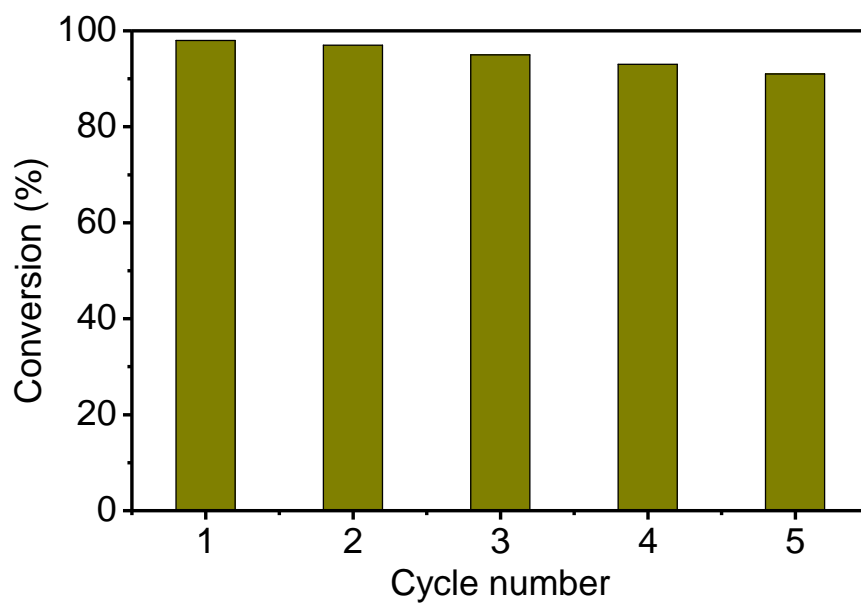


Fig. S10 Reusability data showing the efficiency of Au/g-C₃N₄ nanosheets tested for five successive photocatalytic BA oxidation reactions under sunlight. (The catalysts were recovered by centrifugation, washed with acetonitrile and ethanol and dried at 60 °C before reuse).

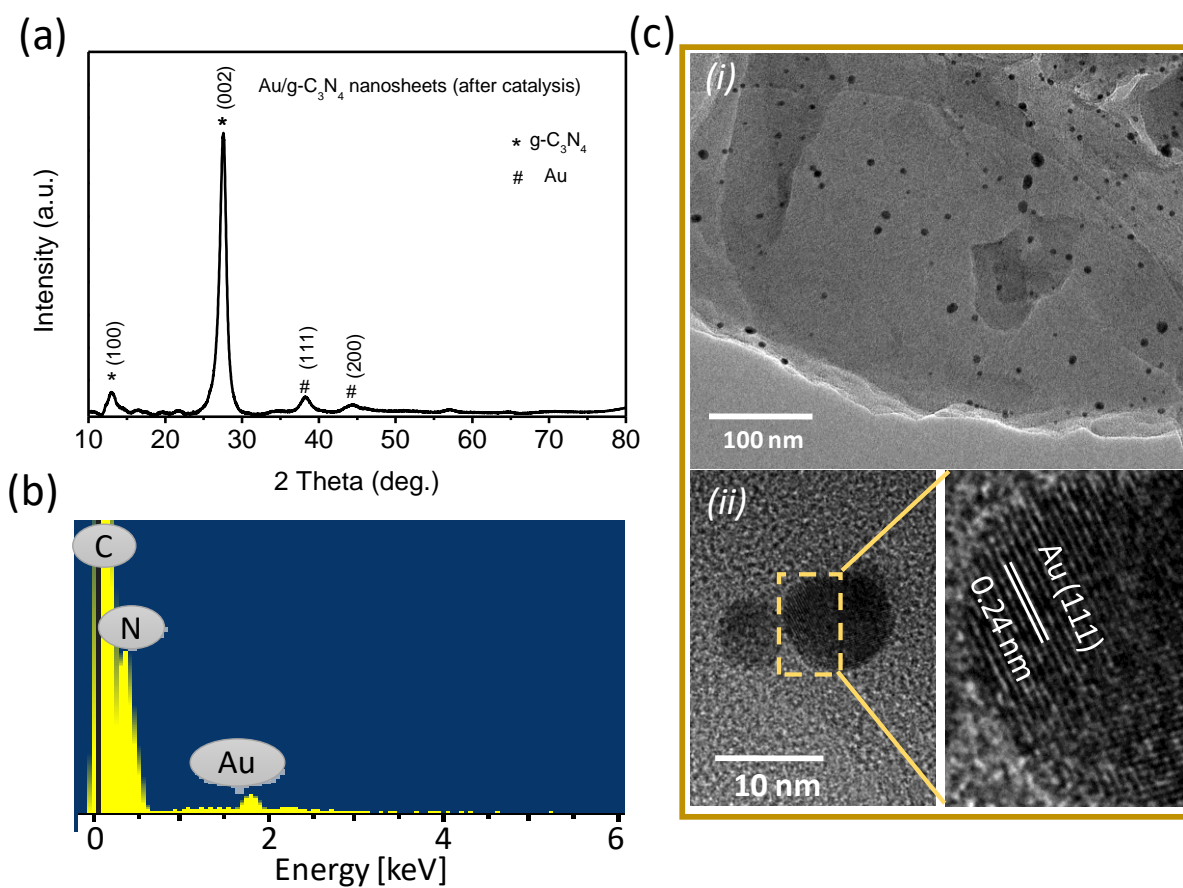


Fig. S11 XRD pattern of the used Au/g-C₃N₄ nanosheets in five successive catalytic cycles. (b) SEM-EDS spectrum of the used Au/g-C₃N₄ nanosheets for catalysis reaction. (c) TEM image (i), HR-TEM image (ii) of the Au/g-C₃N₄ nanosheets obtained after catalysis.

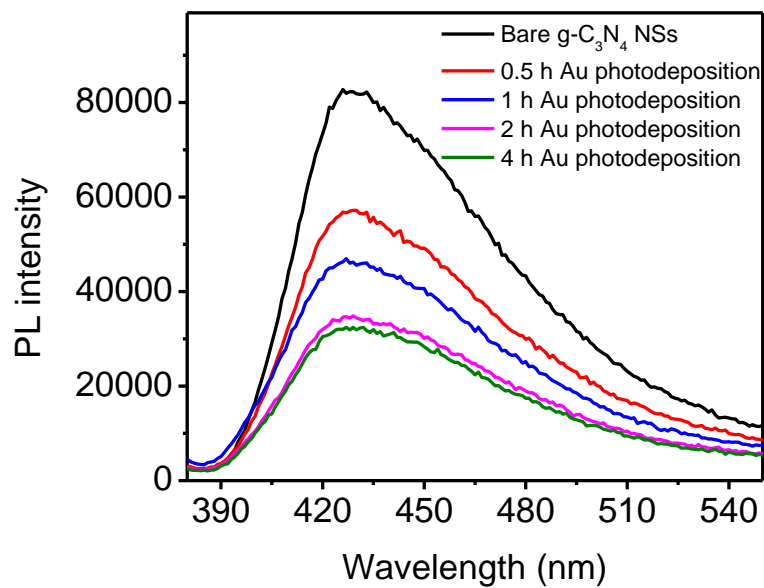


Fig. S12 PL emission spectra of the g-C₃N₄ nanosheets at various times during the Au photo-deposition. The systematic decrease in the PL intensity confirms the transfer of excited electrons from the nanosheets to the Au nanoparticles.

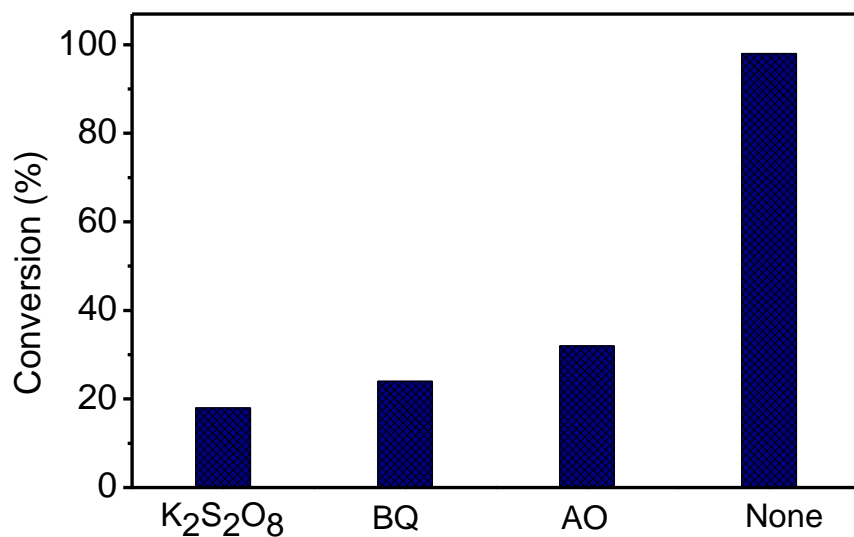


Fig. S13 Role of different scavengers in the photocatalytic BA oxidation. 3.0 mmol of scavengers were used in each set of reaction, keeping all other parameters same.

Note S3. Probable benzyl amine photo-oxidation reaction mechanism:

We recall from the description in the main text that the molecular oxygen acts as a reactant in the benzyl amine oxidation. It was also observed that both excited electrons and holes are responsible for the reaction. Besides the high photocatalytic efficiency arises from both co-catalytic and surface plasmonic effect of the Au NPs. In the co-catalytic event, the valence band electrons of g-C₃N₄ in Au/g-C₃N₄ gets excited upon light irradiation and goes to the conduction band (C.B.) and transfer to the Au Fermi surface. On the other hand, if the particle is exposed to a light frequency corresponding to LSP of the Au NP, the hot electrons generated on it go to the C.B. of the g-C₃N₄. Since this reaction is known to be mediated by radicals generated by transfer of electrons and holes, we have carried out a series of controlled experiments using electron, hole and radical scavengers, as discussed in the main text and represented in Scheme 1. The corresponding elementary steps are as follows:

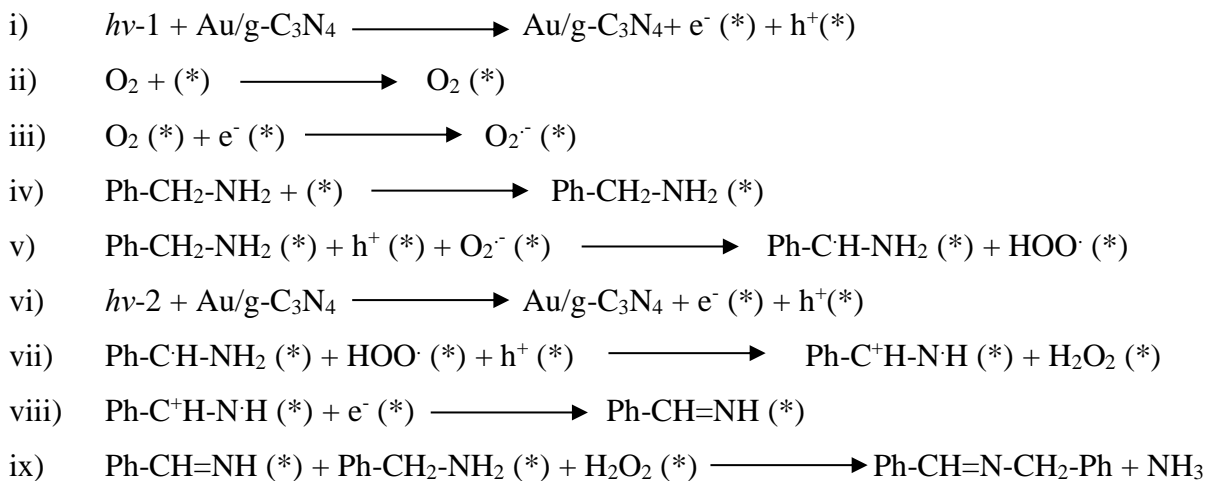


Figure 14

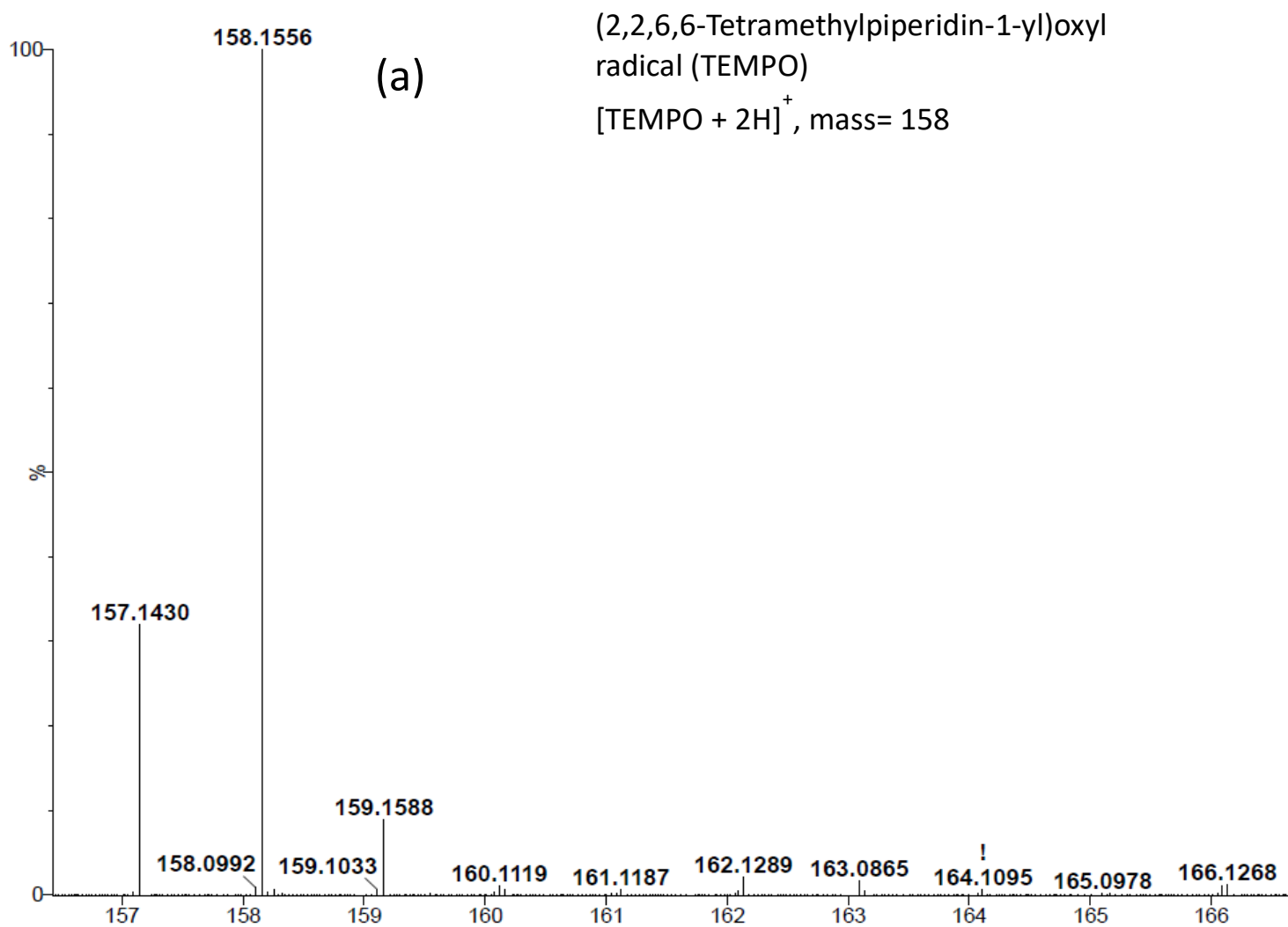


Fig. S14 (HRMS spectra were recorded before starting the experiment and after irradiation with sunlight for 1 h.) (a) [TEMPO+2H]⁺ was observed at the beginning in CH₃CN solvent.³

Figure 14

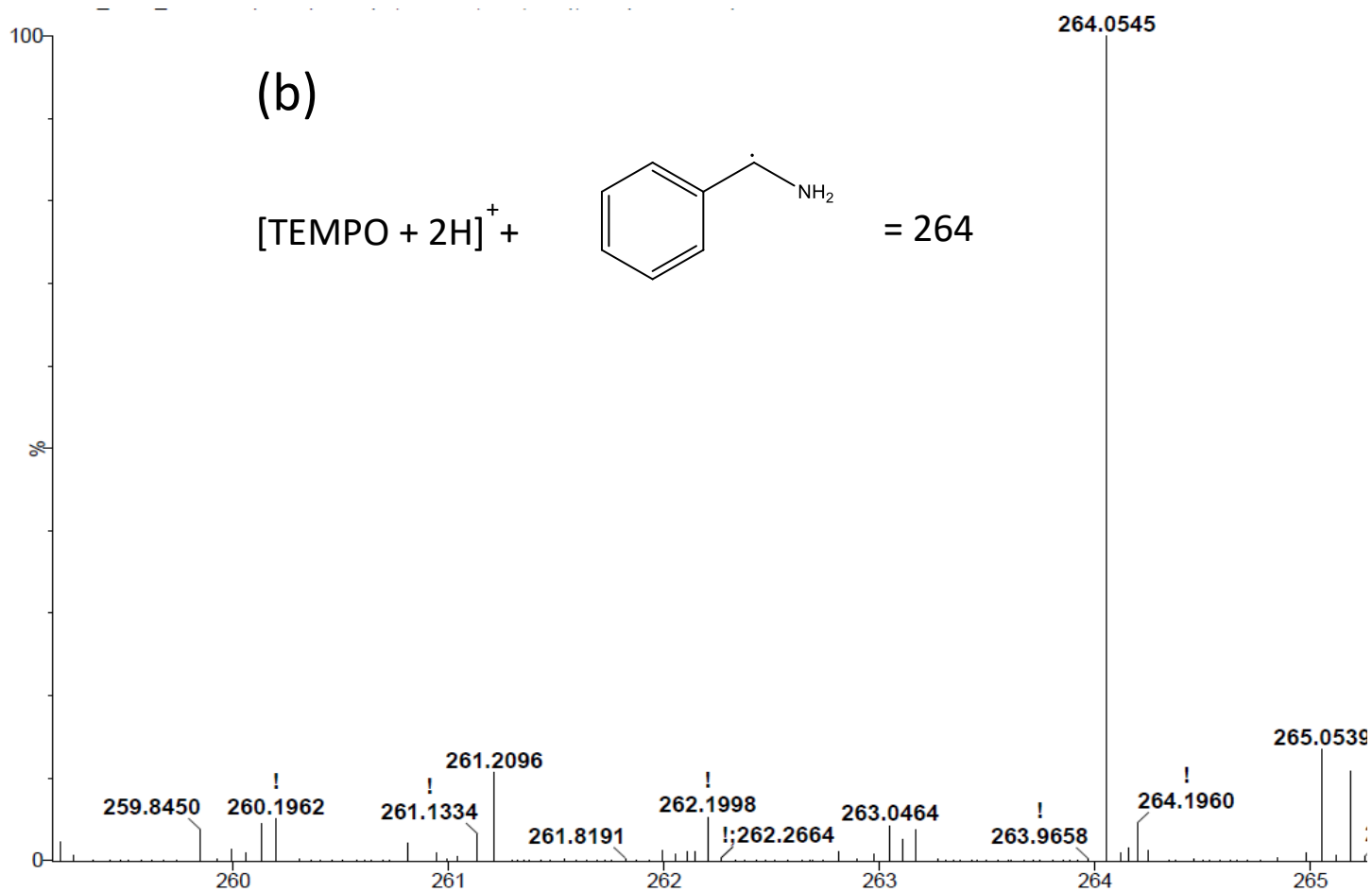


Fig. S14 (HRMS spectra were recorded before starting the experiment and after irradiation with sunlight for 1 h.) (b) TEMPO formed an adduct with the carbon radical species after irradiation with sunlight for 1h.

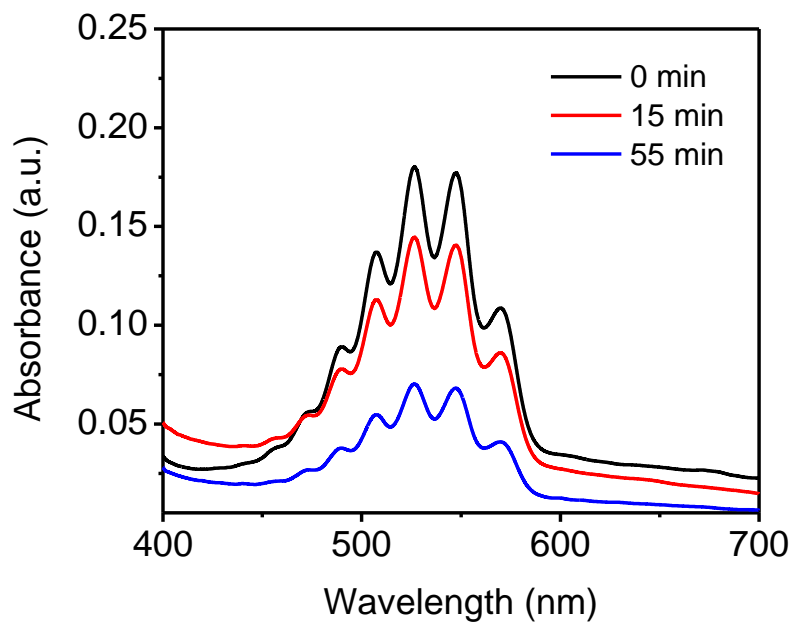
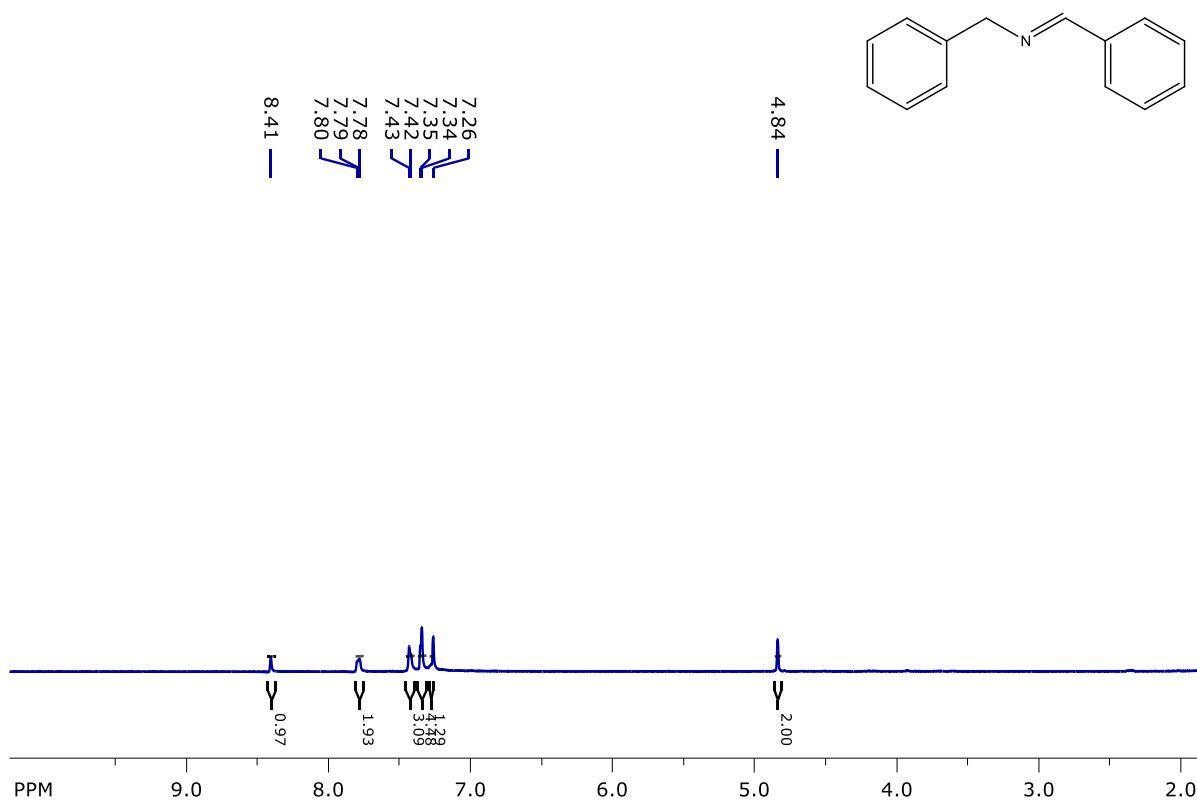


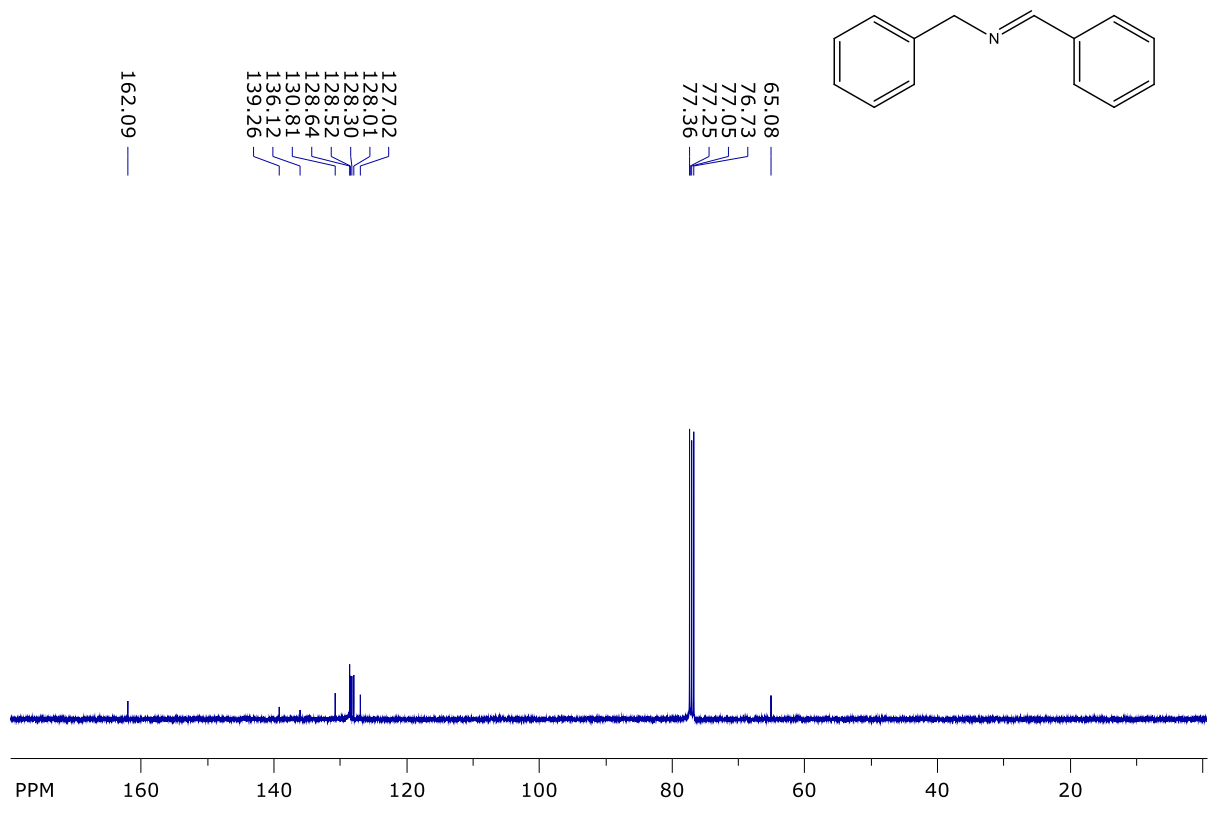
Fig. S15 UV-visible absorption spectra of a KMnO_4 solution after adding reaction aliquots of BA photo-oxidation showing a gradual decrease of absorbance during the reaction due to *in-situ* generation of H_2O_2 .

NMR spectra of various products of amine oxidation reaction

Substrate: Benzylamine

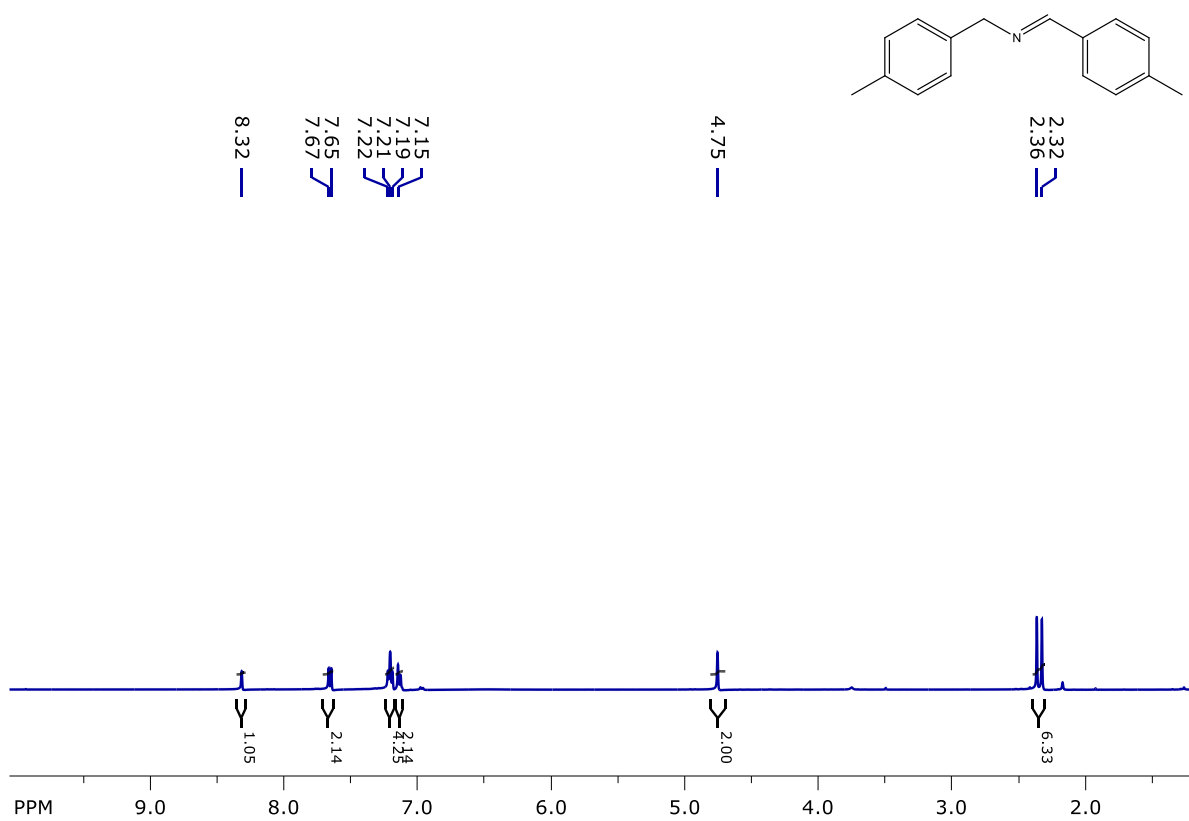


¹H NMR (400MHz, CDCl₃): δ_H 8.41 (s,1H), 7.80-7.78 (m,2H), 7.43-7.26 (m,8H), 4.84 (s,2H)



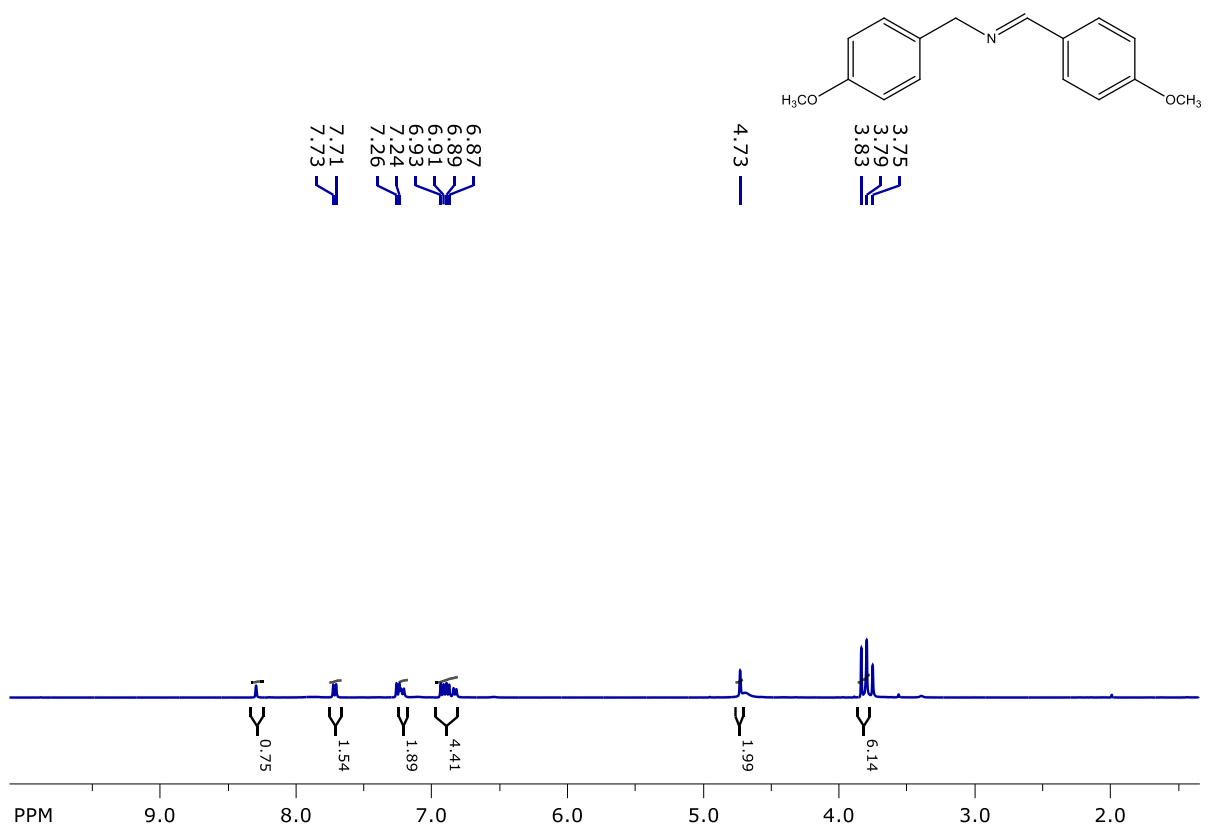
¹³C NMR (400 MHz, CDCl₃): δ_C 162.0, 139.2, 136.2, 130.8, 128.6, 128.5, 128.3, 128.0, 127.0, 65.0.

Substrate: 4-methyl benzylamine



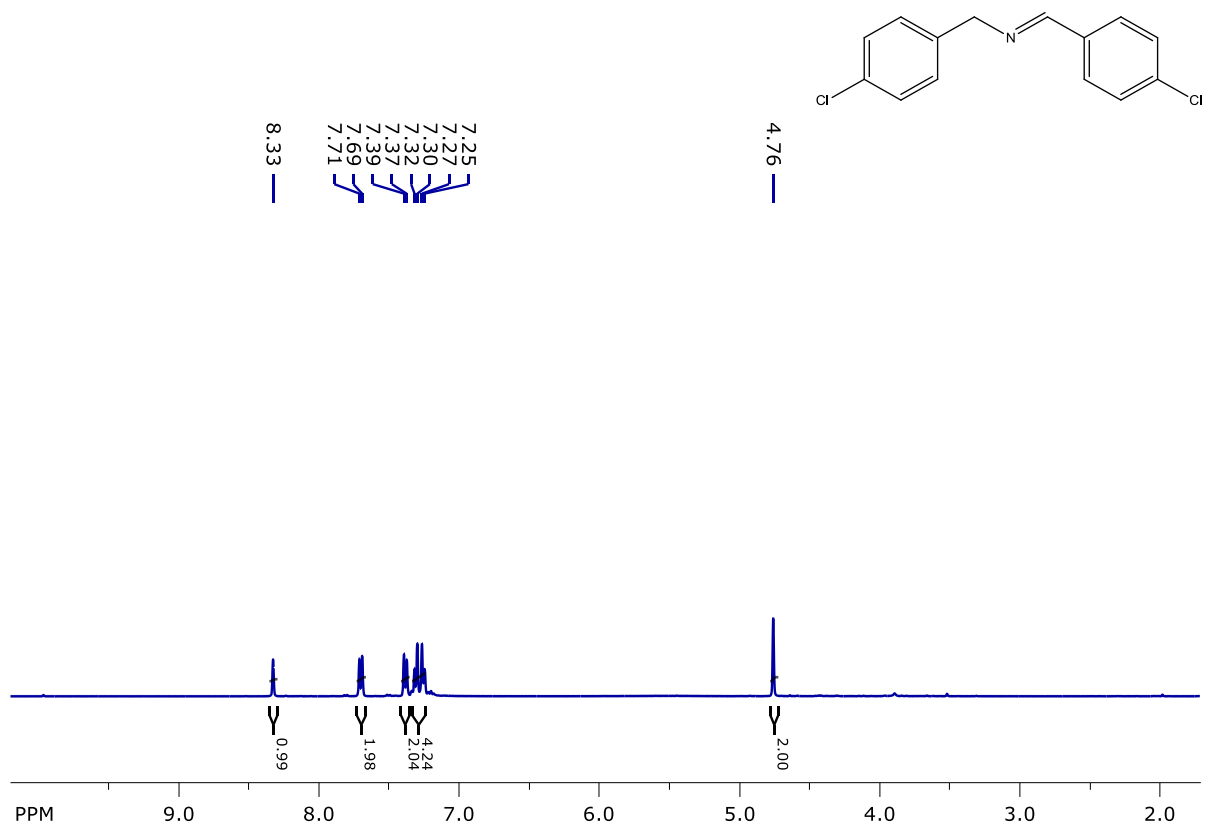
¹H NMR (400 MHz, CDCl₃): δ_H 8.32 (s,1H), 7.65 (d,2H), 7.22-7.15 (m,6H), 4.75 (s,2H), 2.36 (s,3H), 2.32 (s,3H)

Substrate: 4-methoxy benzylamine



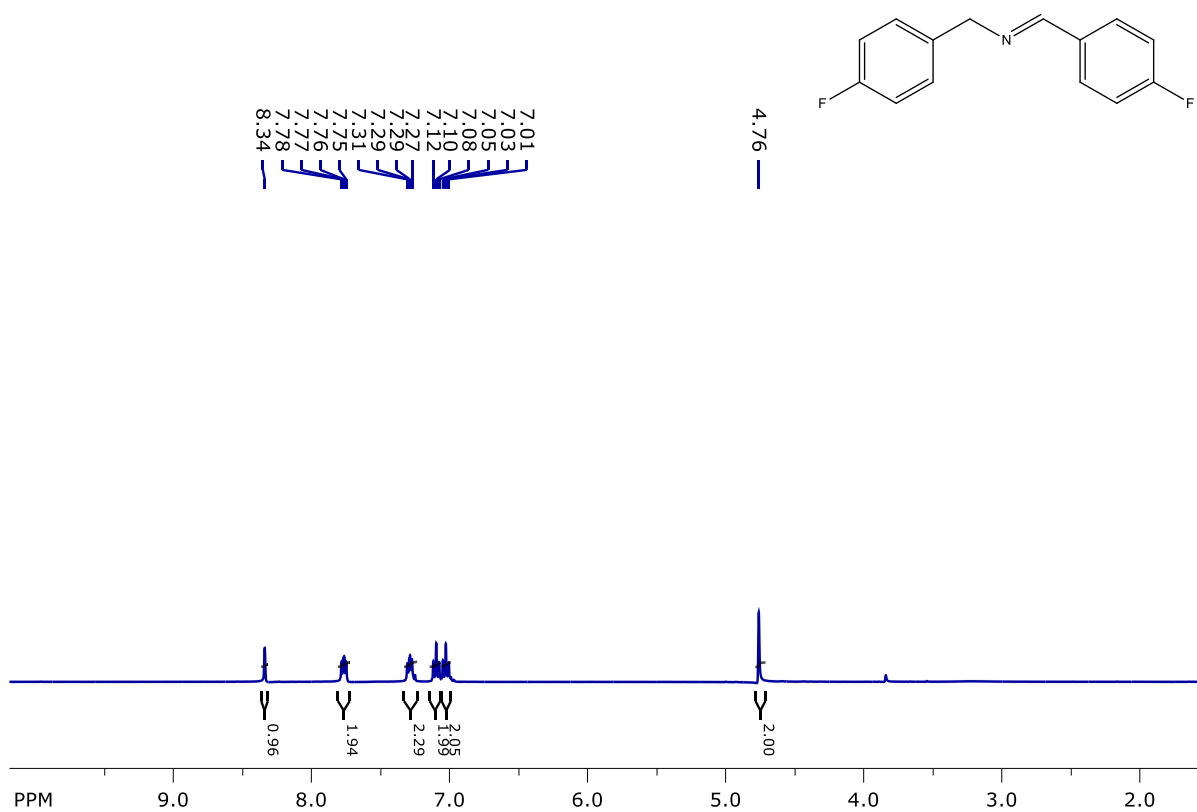
¹H NMR (400 MHz, CDCl₃): δ_H 8.34 (s, 1H), 7.73 (d, 2H), 7.26 (d, 2H), 6.91 (m, 4H), 4.71 (s, 2H), 3.88 (m, 6H).

Substrate: 4-chloro benzylamine



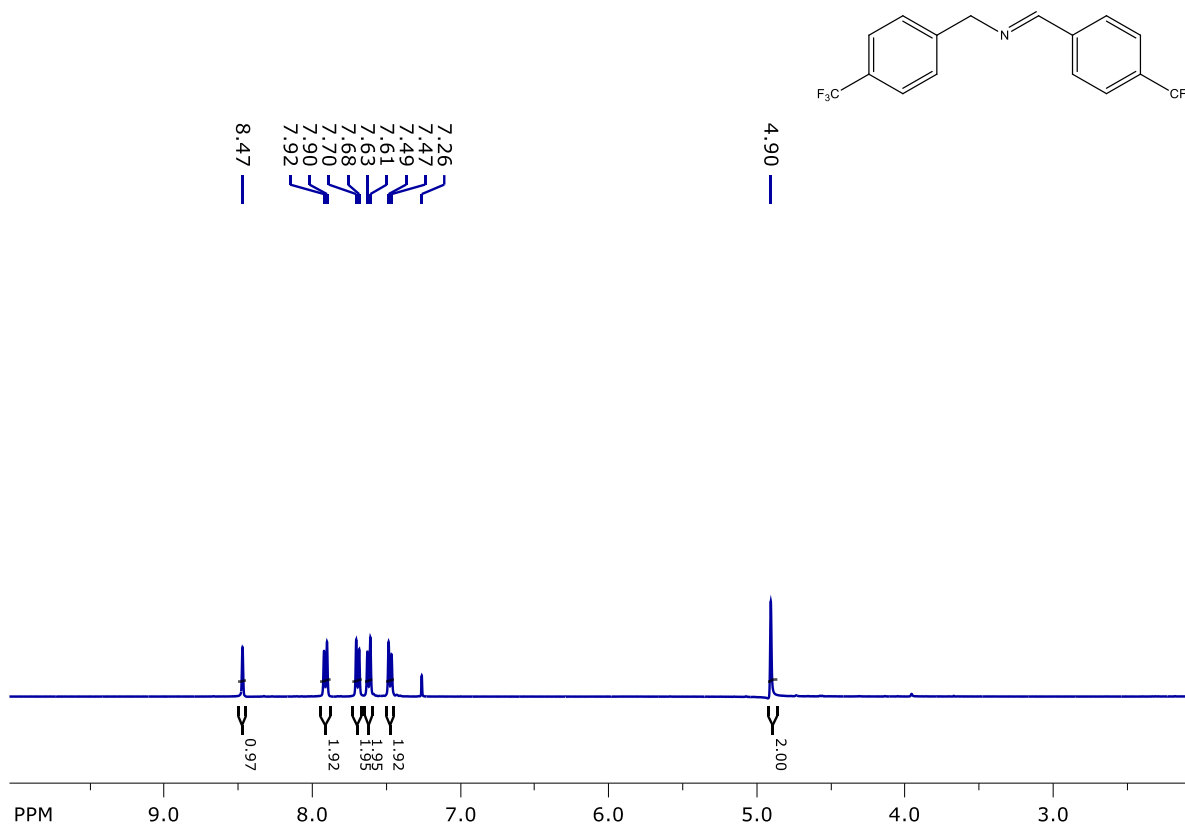
¹H NMR (400MHz, CDCl₃): δ_H 8.33 (s, 1H), 7.71-7.69 (m, 2H), 7.39 (d, 2H), 7.32-7.25 (m, 4H), 4.76 (s, 2H)

Substrate: 4-fluoro benzylamine



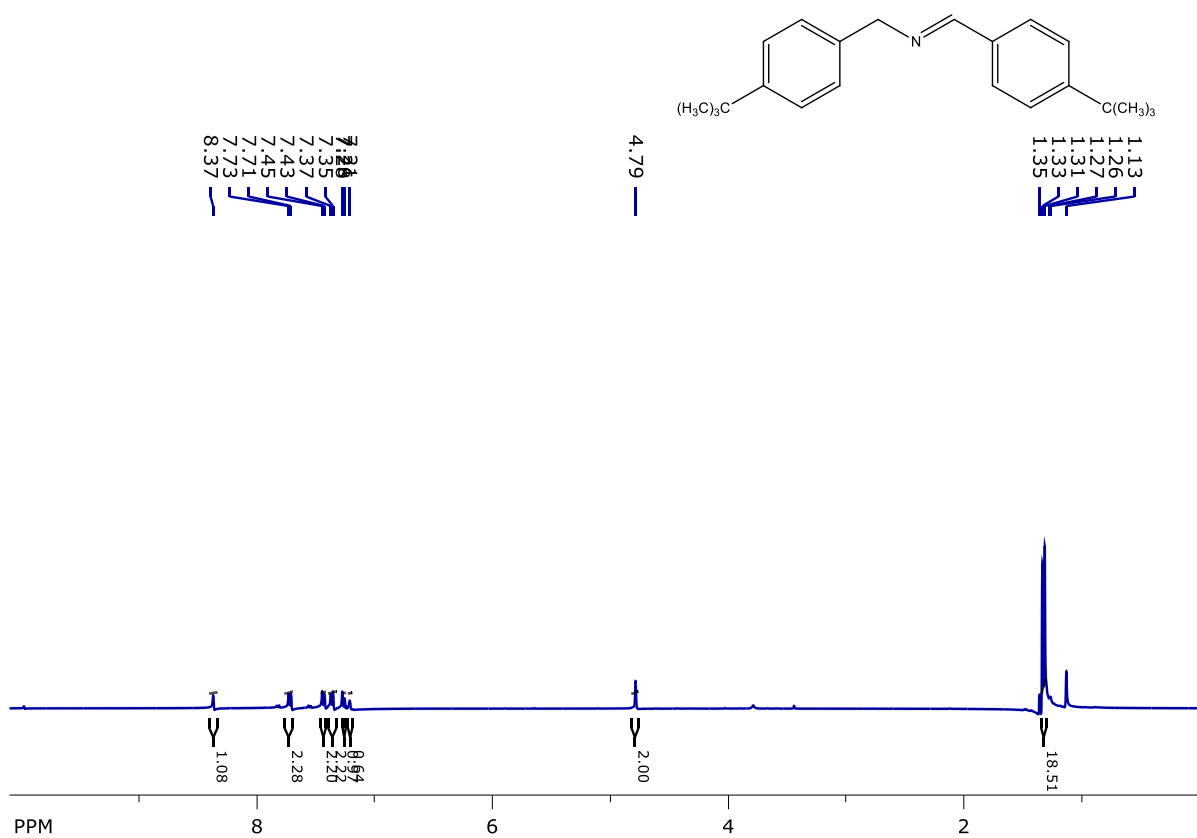
¹H NMR (400 MHz, CDCl₃): δ_H 8.34 (s, 1H), 7.78-7.75 (m, 2H), 7.31-7.29 (m, 2H), 7.12- 7.01 (m, 4H), 4.76(s, 2H)

Substrate: 4-trifluoro methyl benzylamine



¹H NMR (400 MHz, CDCl₃): δ_H 8.47 (s, 1H), 7.92 (d, 2H), 7.70-7.61 (m, 4H), 7.49 (d, 2H), 4.90 (s, 2H)

Substrate: t-butyl benzylamine



^1H NMR (400 MHz, CDCl_3): δ_{H} 8.37 (s, 1H), 7.73-7.71 (m, 2H), 7.45-7.23 (m, 6H), 4.79 (s, 2H), 1.35-1.26 (s, 18H)

Table S1. IR radiation effect on the amine oxidation reaction: Since, natural sun light contain IR radiation, we have performed the following controlled experiments which suggest that the reaction involves a photocatalytic process as the primary process. First, the temperature of the reaction was monitored during the reaction by using a thermometer and found to be almost constant throughout the reaction period (~29-33°C). Second, we have also carried out the reaction in dark, but no conversion was observed, confirming that the process is not purely thermocatalytic and light irradiation is mandatory. Moreover, the high co-catalytic activity below 400 nm where plasmonic heating is expected to be minimal also asserts this fact.

Table S1: Temperature profile of the reaction medium monitored throughout the reaction under sunlight.

Reaction time	20 min	30 min	40 min	50 min	60 min	70 min	80 min	90 min
Temperature (°C)	30	31	30	31	32	29	31	31

Table S2: Comparison of photocatalytic activities for the amine oxidation reaction under ambient conditions by the bulk g-C₃N₄ sample and the NSs.

Material	Reaction time	Conversion (%)
Bulk g-C ₃ N ₄	1.5 h	17
	3 h	26
	6 h	41
g-C ₃ N ₄ NSs	1.5 h	21
	3 h	30
	6 h	52

Table S3: Comparison of BA oxidation activity in this study with other state-of-the-art catalysts.

(**Note:** To compare the efficiency of Au/g-C₃N₄, recent developed highly active catalysts from literatures were selected. However, a comparison is not easy as experimental conditions differ in various studies. Therefore, the reaction parameters such as the catalyst and reactant amount, solvent, reaction atmosphere, time and temperature etc. are included in the table. Among these parameters, purging of O₂ gas during the reaction has high importance since O₂ is the oxidant for the oxidation reaction (see the table below). Entries 14 to 20 demonstrate the effect of temperature on the oxidation reaction). In our study we found that the Au/g-C₃N₄ shows higher oxidation efficiency even at ambient condition in open air.

Sr. No.	Catalyst	Catalyst amount	BA (mmole)	Time (h)	Temp. (°C)	O ₂ /Air	Solvent	Conv. (%)	Select. (%)	Ref.
1.	Au/g-C ₃ N ₄	20 mg	0.5	1.5	r.t	Air	CH ₃ CN	98	>99	Our work
2.	BiVO ₄ /g-C ₃ N ₄	20 mg	0.35	16	r.t	-	CH ₃ CN	87	100	4
3.	[Au ₂₅]/TiO ₂	10 mg	0.2	1.5	r.t	O ₂	CH ₃ CN	98	99	5
4.	Tx-CMP	10 mg	0.5	4	r.t	O ₂	CH ₃ CN	99	91	6
5.	Cd-organic framework	10 mg	0.48	6	r.t	Air	DMF	92	99	7
6.	TiO ₂	50 mg	0.2	4	r.t	O ₂	CH ₃ CN	76	98	8
7.	Mo/Ta/W ternary polyoxometalate	1 mol%	0.2	24	r.t	Air	CH ₃ CN	96	-	9
8.	BiVO ₄	100 mg	0.1	6	r.t	O ₂	CH ₃ CN	99	99	10
9.	Nb ₂ O ₅	100 mg	5	50	r.t	O ₂	Benzene	99	98	11
10.	NH ₂ -MIL-125(Ti)	5 mg	0.1	12	r.t	O ₂	CH ₃ CN	73	86	12
11.	N-doped TiO ₂ @N-doped C	10 mg	0.2	15	r.t	O ₂	CH ₃ CN	99	-	13
12.	TiO ₂ nano-flower	-	-	2	r.t	O ₂	CH ₃ CN	75	70	14
13.	BiOBr	100 mg	0.1	14	r.t	O ₂	CH ₃ CN	100	100	15
14.	Au/CeO ₂	-	0.2	6	100	O ₂	1,4 dioxane	96	97	16
15.	Au/Al ₂ O ₃	100 mg	0.2	24	100	O ₂	Toluene	92	-	17
16.	Fe based MOF	75 mg	4.8	24	100	O ₂	-	67	97	18
17.	WS ₂ NS	-	0.1	30	50	O ₂	CH ₃ CN	92	95	19
18.	Cu-graphene	100 mg	1	6	40	O ₂	CH ₃ CN	99	93	20
19.	CQDs	25 mg	-	12	90	O ₂	-	-	-	21
20.	mpg-C ₃ N ₄	50 mg	1	2	80	O ₂	CH ₃ CN	60	99	22

References:

- 1 B. Jürgens, E. Irran, J. Senker, P. Kroll, H. Müller and W. Schnick, *J. Am. Chem. Soc.*, 2003, **125**, 10288–10300.
- 2 S. R. Lingampalli, U. K. Gautam and C. N. R. Rao, *Energy Environ. Sci.*, 2013, **6**, 3589–3594.
- 3 A. Marjasvaara, M. Torvinen and P. Vainiotalo, *J. Mass Spectrom.*, 2004, **39**, 1139–1146.
- 4 S. Samanta, S. Khilari, D. Pradhan and R. Srivastava, *ACS Sustain. Chem. Eng.*, 2017, **5**, 2562–2577.
- 5 H. Chen, C. Liu, M. Wang, C. Zhang, N. Luo, Y. Wang, H. Abroshan, G. Li and F. Wang, *ACS Catal.*, 2017, **7**, 3632–3638.
- 6 V. R. Battula, H. Singh, S. Kumar, I. Bala, S. K. Pal and K. Kailasam, *ACS Catal.*, 2018, **8**, 6751–6759.
- 7 J. Shi, J. Zhang, T. Liang, D. Tan, X. Tan, Q. Wan, X. Cheng, B. Zhang, B. Han, L. Liu, F. Zhang and G. Chen, *ACS Appl. Mater. Interfaces*, 2019, **11**, 30953–30958.
- 8 X. Lang, W. Ma, Y. Zhao, C. Chen, H. Ji and J. Zhao, *Chem. – A Eur. J.*, 2012, **18**, 2624–2631.
- 9 S. Li, G. Li, P. Ji, J. Zhang, S. Liu, J. Zhang and X. Chen, *ACS Appl. Mater. Interfaces*, 2019, **11**, 43287–43293.
- 10 B. Yuan, R. Chong, B. Zhang, J. Li, Y. Liu and C. Li, *Chem. Commun.*, 2014, **50**, 15593–15596.
- 11 S. Furukawa, Y. Ohno, T. Shishido, K. Teramura and T. Tanaka, *ACS Catal.*, 2011, **1**, 1150–1153.
- 12 D. Sun, L. Ye and Z. Li, *Appl. Catal. B Environ.*, 2015, **164**, 428–432.
- 13 F. Wang, X. He, L. Sun, J. Chen, X. Wang, J. Xu and X. Han, *J. Mater. Chem. A*, 2018, **6**, 2091–2099.
- 14 J. Bu, J. Fang, W. R. Leow, K. Zheng and X. Chen, *RSC Adv.*, 2015, **5**, 103895–103900.
- 15 A. Han, H. Zhang, G.-K. Chuah and S. Jaenicke, *Appl. Catal. B Environ.*, 2017, **219**, 269–275.
- 16 M. Wang, F. Wang, J. Ma, M. Li, Z. Zhang, Y. Wang, X. Zhang and J. Xu, *Chem. Commun.*, 2014, **50**, 292–294.
- 17 B. Zhu, M. Lazar, B. G. Trewyn and R. J. Angelici, *J. Catal.*, 2008, **260**, 1–6.
- 18 A. Dhakshinamoorthy, M. Alvaro and H. Garcia, *ChemCatChem*, 2010, **2**, 1438–1443.
- 19 F. Raza, J. H. Park, H.-R. Lee, H.-I. Kim, S.-J. Jeon and J.-H. Kim, *ACS Catal.*, 2016, **6**, 2754–2759.
- 20 Z.-Y. Zhai, X.-N. Guo, G.-Q. Jin and X.-Y. Guo, *Catal. Sci. Technol.*, 2015, **5**, 4202–4207.
- 21 J. Ye, K. Ni, J. Liu, G. Chen, M. Ikram and Y. Zhu, *ChemCatChem*, 2018, **10**, 259–265.
- 22 F. Su, S. C. Mathew, L. Möhlmann, M. Antonietti, X. Wang and S. Blechert, *Angew. Chemie Int. Ed.*, 2011, **50**, 657–660.